

# Temperature dependence of single-particle properties in isospin symmetric and asymmetric matter within the Dirac-Brueckner-Hartree-Fock model

Francesca Sammarruca

*Physics Department, University of Idaho, Moscow, ID 83844-0903, U.S.A \**  
(Dated: June 10, 2010)

The understanding of the interaction of nucleons in nuclear and neutron-rich matter at non-zero temperature is important for a variety of applications ranging from heavy-ion collisions to nuclear astrophysics. In this paper we apply the Dirac-Brueckner-Hartree-Fock method along with the Bonn B potential to predict single-particle properties in symmetric nuclear matter and neutron-rich matter at finite temperature. It is found that temperature effects are generally small but can be significant at low density and momentum.

## I. INTRODUCTION

The nuclear equation of state (EoS) at finite temperature is of fundamental importance for heavy-ion (HI) physics [1] as well as nuclear astrophysics, particularly in the final stages of a supernova evolution. Knowledge of the finite-temperature EoS can be of great help in the interpretation of experiments aimed at identifying a liquid-gas phase transition. Presently, findings concerning such transition are very model dependent [2–8].

When other aspects, such as spin asymmetries of nuclear/neutron matter are included as well, conclusions are even more contradictory. For instance, the influence of finite temperature on the manifestation of ferromagnetic instabilities is an unsettled question. In Ref. [9], phenomenological Skyrme-type interactions are used in a Hartree-Fock scheme. It is found that the critical density for ferromagnetism decreases with temperature. On the other hand, in Ref. [10] the authors report no indication of ferromagnetic instability at any density or temperature based on the Brueckner-Hartree-Fock (BHF) approximation and the Argonne V18 nucleon-nucleon (NN) interaction [11]. The properties of spin-polarized neutron matter at finite temperature are studied in Ref. [12] with two different parameterizations of the Gogny interaction. The results show two qualitatively different behaviors for the two parameterizations. The reasons for these discrepancies must be carefully studied and their origin understood in terms of specific features of the nuclear force and/or the chosen many-body framework.

Previous work on the temperature dependence of the EoS includes the calculations by Baldo and Ferreira who used the Bloch-De Dominicis diagrammatic expansion [13], Brueckner-Hartree-Fock calculations with and without three-body forces (TBF) [2], and the predictions of Ref. [14] based on the Green's function method. Investigations of the finite temperature EoS have also been performed within the relativistic Hartree approximation [15–21], whereas the relativistic Hartree-Fock approach

was applied in Refs. [21].

The entropy per particle in symmetric nuclear matter has been studied in Ref. [22] within the self-consistent Green's function (SCGF) approach, where both particle-particle and hole-hole scatterings are included. The SCGF framework allows direct access to the single-particle spectral function and thus to all the one-body properties of the system. A most recent work by Rios *et al.* [23] addresses hot neutron matter within the same approach and performs a comparison with other models. Hot asymmetric matter and  $\beta$ -stable matter have been studied by Moustakidis *et al.* [24, 25] using temperature and momentum dependent effective interactions. An earlier calculation with the DBHF method can be found in Ref. [7]. Also, Ref. [8] contains a study of isospin asymmetric matter based on the DBHF approach.

The study of the many EoS-related aspects in both symmetric and neutron-rich matter starting from realistic NN forces and within a microscopic model is still a considerable challenge. It is the purpose of this paper to report the first part of a comprehensive study of temperature dependence of nuclear and neutron-rich matter properties based on the Dirac-Brueckner-Hartree-Fock (DBHF) approach. Here, we will concentrate on the properties of the single-particle within the nuclear medium for the following reason: although the nuclear/neutron matter energy density is certainly an important quantity, the single-particle interaction and its temperature dependence, which determine the one-body properties in the medium, are perhaps more relevant for non-equilibrium processes such as relativistic heavy-ion collisions.

Previously, we have confronted isospin asymmetries [26, 27] as well as spin asymmetries [28] effects on the equation of state of cold matter. In this work, we have extended the isospin-asymmetric matter calculation of Ref. [26] to include finite temperature effects. The simultaneous consideration of isospin asymmetry and temperature dependence will make our microscopic predictions more broadly useful and capable to reach out to the properties of the hot environment present in the latest stage of a supernova collapse or in the collision of heavy nuclei at intermediate energies. Starting from the present

---

\*Electronic address: fsammarr@uidaho.edu

baseline, we plan to address, in future work, additional aspects such as temperature dependence of in-medium effective cross sections and hot spin asymmetric matter.

Next, after a review of the main aspects of the formalism, we will show and discuss predictions of the chemical potential and single-particle properties in symmetric and pure neutron matter. In Section **IIIC** we show a typical set of predictions for the single-neutron and single-proton potentials in isospin-asymmetric matter.

Hot nuclear and neutron-rich matter are infinite fermionic systems where only the strong interactions among nucleons are taken into account. The temperatures typically considered are of a few tens of MeV, relatively small on the scale of nuclear energies. For instance, close to the saturation density of nuclear matter, the free Fermi energy,  $e_F$ , is approximately 40-50 MeV, and thus a temperature of 20 MeV is still somewhat low, with  $T/e_F \sim 0.5$ .

## II. FORMALISM

Within the DBHF method, the interactions of the nucleons with the nuclear medium are expressed as self-energy corrections to the nucleon propagator. That is, the nucleons are regarded as “dressed” particles, essentially a gas of non-interacting quasi-fermions. The behavior of the dressed nucleon is determined by the effective nucleon propagator, which obeys the Dyson equation. Relativistic effects lead to an intrinsically density-dependent interaction which is consistent with the contribution from TBF typically employed in non-relativistic approaches. The advantage of the DBHF approximation is the absence of phenomenological TBF to be extrapolated at higher densities from their values determined through observables at normal density.

In the quasi-particle approximation, the transition to the temperature-dependent case is introduced by replacing the zero-temperature occupation number with its finite-temperature counterpart, namely the Fermi-Dirac occupation density. In fact, it can be shown that the zero-temperature terms in the Bethe-Goldstone expansion where temperature is introduced in the occupation number only are the dominant ones [13], thus justifying this simplified procedure. More specifically, one replaces

$$n(k, \rho) = \begin{cases} 1 & \text{if } k \leq k_F \\ 0 & \text{otherwise} \end{cases}, \quad (1)$$

with the Fermi-Dirac distribution

$$n_{FD}(k, \rho, T) = \frac{1}{1 + e^{(\epsilon(k, \rho, T) - \mu(\rho, T))/T}}. \quad (2)$$

Here  $T$  is the temperature in MeV,  $\epsilon(k, \rho, T)$  the single-particle energy, function of momentum, density, and temperature, and  $\mu$  the chemical potential, to be determined. The angle-averaged Pauli operator is evaluated numeri-

cally. It's given by

$$Q(q, P, \rho, T) = \frac{1}{2} \int_{-1}^{+1} d(\cos \theta) (1 - n_{FD}(k, \rho, T)) \times \\ \times (1 - n_{FD}(k', \rho, T)), \quad (3)$$

for two nucleons with momenta  $\vec{k}$  and  $\vec{k}'$ , with relative and total momentum given by  $\vec{q} = \frac{\vec{k} - \vec{k}'}{2}$  and  $\vec{P} = \vec{k} + \vec{k}'$ , respectively.

The single-particle energy,  $\epsilon(k, \rho, T)$ , is now temperature dependent. It can be obtained self-consistently with the Dirac states following the same procedure as used in the zero temperature case, but including Eq. (2) in the calculation of the single-particle potential. At each iteration of the self-consistent calculation, the normalization condition

$$\rho = D \frac{1}{(2\pi)^3} \int_0^\infty n_{FD}(k, \rho, T) d^3k, \quad (4)$$

allows to extract the microscopic chemical potential,  $\mu(\rho, T)$ .  $D$  is a degeneracy factor, equal to 4 for symmetric unpolarized nuclear matter or 2 for unpolarized neutron matter. For isospin-asymmetric matter, proton and neutron densities are fitted simultaneously, see Eq. (15).

In close analogy with the  $T = 0$  case, the single-particle potential and the self-consistent nucleon-nucleon  $G$ -matrix are related by

$$U(\vec{k}, \rho, T) = \sum_{I, L, S, J} \frac{(2I+1)(2J+1)}{(2t+1)(2s+1)} \times \\ \times \int_0^\infty n_{FD}(k', \rho, T) G_{NN}^{T, L, S, J}(q(\vec{k}, \vec{k}'), P(\vec{k}, \vec{k}')) d^3k', \quad (5)$$

where  $I, L, S$ , and  $J$  are the NN system quantum numbers while  $s$  and  $t$  are the single-particle spin and isospin, respectively. Integrations over the Fermi sea are performed using a cutoff adjusted to the density. We found a value of 6 fm to be sufficient for the highest densities and temperatures considered here.

The single-particle energy is the sum of potential ( $U$ ) and kinetic ( $K$ ) energy contributions,

$$\epsilon(k, \rho, T) = U(k, \rho, T) + K(k, \rho, T). \quad (6)$$

It is parametrized using the same *ansatz* as in the  $T = 0$  case [29] for a spin-symmetric, rotationally invariant system:

$$\epsilon(k, \rho, T) = \sqrt{k^2 + (m^*)^2} + U_V, \quad (7)$$

where  $U_V$  is the time-like part of the vector potential and  $m^* = m + U_S$ , with  $U_S$  the scalar potential, now both density and temperature dependent. This quantity plays an important role in temperature and momentum-dependent transport models of heavy-ion collisions.

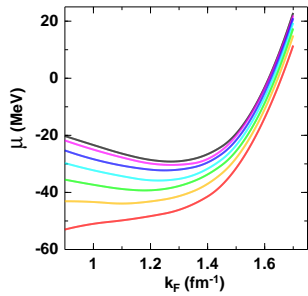


FIG. 1: (color online) The chemical potential in symmetric matter as a function of the Fermi momentum at various temperatures from  $T = 0$  to  $T = 30$  MeV in steps of 5 MeV. The chemical potential decreases with temperature.

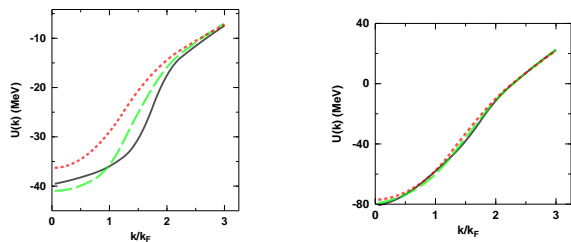


FIG. 2: (color online) The single-particle potential in symmetric matter as a function of the momentum for three different temperatures:  $T = 0$  (solid black);  $T = 10$  (dashed green);  $T = 20$  (dotted red). The left and right panels correspond to Fermi momenta equal to  $0.9 \text{ fm}^{-1}$  and  $1.3 \text{ fm}^{-1}$ , respectively.

Once a self-consistent solution is obtained for the single-particle potential, and, simultaneously, for the chemical potential, the entropy/particle can be calculated, along with all thermodynamic quantities. In the mean-field approximation, the entropy/particle is given by

$$S = -\frac{1}{\rho} \frac{D}{(2\pi)^3} \int_0^\infty [n_{FD}(k, \rho, T) \ln n_{FD}(k, \rho, T) + (1 - n_{FD}(k, \rho, T)) \ln (1 - n_{FD}(k, \rho, T))] d^3k, \quad (8)$$

that is, it has the same functional form as in a noninteracting system.

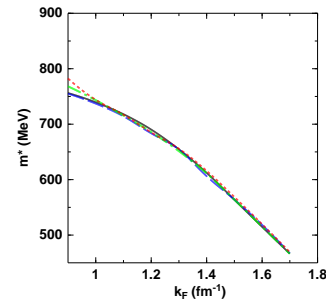


FIG. 3: (color online) Effective mass in symmetric matter as a function of the Fermi momentum and for different temperatures:  $T = 0$  (solid black);  $T = 10$  (dashed blue);  $T = 15$  (dash-dotted green);  $T = 20$  (dotted red).

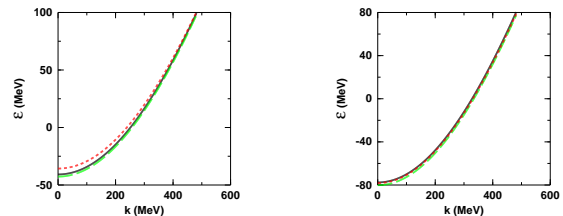


FIG. 4: (color online) The single-particle energy minus the rest mass in symmetric matter parametrized as in Eq. (7) vs. the momentum at different temperatures:  $T = 0$  (solid black);  $T = 10$  (dashed green);  $T = 20$  (dotted red). The left and right panels correspond to Fermi momenta equal to  $0.9 \text{ fm}^{-1}$  and  $1.3 \text{ fm}^{-1}$ , respectively.

### III. RESULTS

#### A. Symmetric Nuclear Matter

We begin by showing the predicted chemical potential in symmetric nuclear matter (SNM), see Fig. 1. Each curve is an isotherm starting from zero temperature and going up to  $T = 30$  MeV in steps of 5 MeV ( $\mu$  goes down with increasing temperature). The effect of temperature is definitely larger at the lower densities and increases in size with increasing temperature. Our predictions are in fair qualitative agreement with those shown in Ref. [13], with or without the contribution of TBF, which do not seem to have a major effect on the chemical potential.

Next, we show the single-particle potential in SNM,  $U(k, \rho, T)$ , see Fig. 2. The effect of temperature is much more pronounced at low density (compare left and right panels) and low momenta. The general tendency is to turn slightly more repulsive with increasing temperature, although this trend becomes clear only at the higher tem-

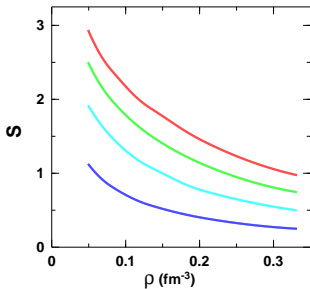


FIG. 5: (color online) The entropy/particle in SNM as a function of density and for increasing temperatures of  $T = 5, 10, 15$ , and  $20$  MeV. The entropy increases with temperature.

perature. The increased repulsion is the result of a combination of effects. Temperature “smears out” the step function distribution, Eq. (1), so that the interaction probability increases (decreases) at low (high) momenta due to the smaller (larger) occupation probability as compared to the  $T = 0$  case. Although Pauli blocking is generally reduced by temperature (which suggests increased attraction among the particles), the integral in Eq. (5) receives contributions from  $G$ -matrix elements at higher momenta (as compared to the zero temperature case), and such contributions tend to be repulsive. In the end, we observe a net effect that is repulsive, except at the lowest temperatures, and essentially negligible at high momenta. In Ref. [7] the equivalent Schrodinger optical potential was constructed from the Dirac self-energies and found to be remarkably insensitive to temperature.

Consistent with Fig. 2, the temperature dependence of the effective mass is generally small, see Fig. 3, and more noticeable at low density. Thus, in the range of densities and temperatures considered here, we expect only minor effects on the in-medium cross sections, whose behavior is essentially dominated by the effective mass. A slightly repulsive temperature effect on the DBHF effective mass was found in Ref. [7] as well.

The single-particle energy, not including the rest mass, is shown in Fig. 4 at fixed density and for different temperatures. Fig. 4 confirms that the single-particle interaction is noticeably impacted only at the lowest momenta.

We conclude this set of results by showing the entropy/particle, which is a measure of thermal disorder. Entropy production in multifragmentation events in heavy-ion collisions is a crucial quantity in the determination of the mass fragment distribution. The entropy per particle is shown in Fig. 5 as a function of density and for various temperatures, and in Fig. 6 it is displayed as a function of temperature at a fixed density (close to saturation density). The entropy increases with temperature, as physically reasonable, and decreases substantially with density. At low  $T$ , it is expected to approach a linear de-

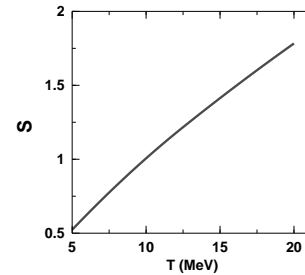


FIG. 6: The entropy/particle in SNM as a function of temperature at a density corresponding to a Fermi momentum of  $1.3 \text{ fm}^{-1}$ .

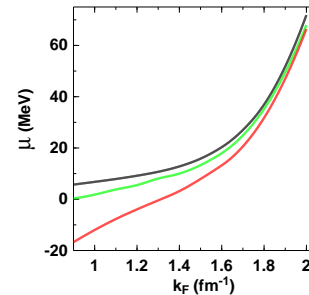


FIG. 7: (color online) The chemical potential in neutron matter as a function of the Fermi momentum at  $T = 0, 10$ , and  $20$  MeV. The chemical potential decreases with temperature.

pendence due to the fact that, for a Fermi liquid, the relation between  $S$  and  $T$  should be approximately

$$S \approx \frac{\pi^2}{3\rho} N(T=0)T, \quad (9)$$

in terms of the density of states at the Fermi surface.

Although weak model dependence is not a general feature of thermodynamic quantities, the authors of Ref. [22] demonstrate that different approximations to the entropy, including the quasi-particle approximation in the temperature dependent BHF scheme, differ from each other by 10 to 20% at most. This may be due to cancellations in the difference between the single-particle energy and the chemical potential [22].

## B. Neutron Matter

We have done a similar study of hot neutron matter (NM) as well. The chemical potential in NM is shown

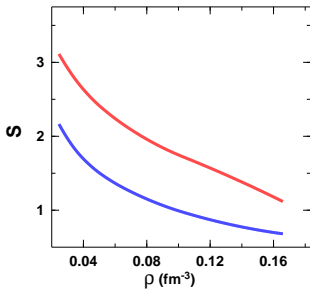


FIG. 8: (color online) The entropy/particle in NM as a function of density at  $T = 10$  (lower curve) and  $20$  MeV (upper curve).

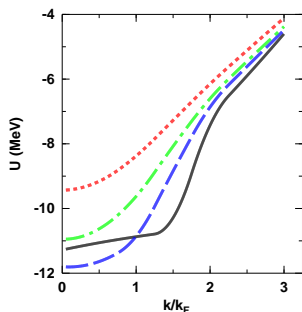


FIG. 9: (color online) The single-particle potential in neutron matter as a function of the momentum at different temperatures:  $T = 0$  (solid black);  $T = 10$  (dashed blue);  $T = 20$  (dash-dotted green);  $T = 30$  (dotted red). The neutron matter Fermi momentum is equal to  $0.9 \text{ fm}^{-1}$ .

in Fig. 7 as a function of the Fermi momentum. (Of course, the same Fermi momentum corresponds to half the density as compared to SNM.) The *microscopic* chemical potential, as obtained from the normalization condition Eq. (4), was shown to be in good agreement with the *macroscopic* one, obtained from the bulk properties through the derivative of the free energy density [23].

The entropy in NM is displayed in Fig. 8. As for the case of SNM, discrepancies between predictions from different models have been found to be small, especially those arising from the use of different NN potential models [23]. In fact, our predictions (based on the Bonn B potential) are close to those shown in Ref. [23] either with CDBONN [30] or Argonne V18 [11]. Concerning different many-body approaches, there are indications that contributions to the entropy from dynamical correlations (which would fragment the quasiparticle peak) are small. Hence, different predictions tend to approach the “dy-

namical quasiparticle” result [23].

The temperature dependence of the single-particle interaction in hot NM is comparable to, or smaller than, the one encountered in the SNM case. We show a representative case in Fig. 9. It is interesting to notice, from Fig. 9 and from the left panel in Fig. 2, how there is a tendency of the potential to become deeper at first and then more shallow as the temperature increases. Also, temperature appears to “wash out” some of the structure in the potential.

### C. Isospin-asymmetric matter

The isospin splitting of the nucleon mean field in isospin-asymmetric matter is a topic of great contemporary interest. It gives rise to the symmetry potential, a quantity which plays a crucial role in simulations of heavy-ion collisions (see Ref. [27] and references therein).

We have incorporate temperature dependence in our calculation of isospin-asymmetric nuclear matter (IANM) [26, 27]. Asymmetric nuclear matter can be characterized by the neutron density,  $\rho_n$ , and the proton density,  $\rho_p$ . In infinite matter, they are obtained by summing the neutron or proton states per volume (up to their respective Fermi momenta,  $k_F^n$  or  $k_F^p$ ) and applying the appropriate degeneracy factor. The result is

$$\rho_i = \frac{(k_F^i)^3}{3\pi^2}, \quad (10)$$

with  $i = n$  or  $p$ . It is more convenient to refer to the total density  $\rho = \rho_n + \rho_p$  and the asymmetry (or neutron excess) parameter  $\alpha = \frac{\rho_n - \rho_p}{\rho}$ . Clearly,  $\alpha=0$  corresponds to symmetric matter and  $\alpha=1$  to neutron matter. In terms of  $\alpha$  and the average Fermi momentum,  $k_F$ , related to the total density in the usual way,

$$\rho = \frac{2k_F^3}{3\pi^2}, \quad (11)$$

the neutron and proton Fermi momenta can be expressed as

$$k_F^n = k_F(1 + \alpha)^{1/3} \quad (12)$$

and

$$k_F^p = k_F(1 - \alpha)^{1/3}, \quad (13)$$

respectively. The formulas given in Section II are extended to include two types of fermions. For instance,

$$Q_{\tau,\tau'}(q, P, \rho, \alpha, T) = \frac{1}{2} \int_{-1}^{+1} d(\cos \theta) (1 - n_{FD,\tau}(k_1, \rho, \alpha, T)) \times \\ \times (1 - n_{FD,\tau'}(k_2, \rho, \alpha, T)), \quad (14)$$

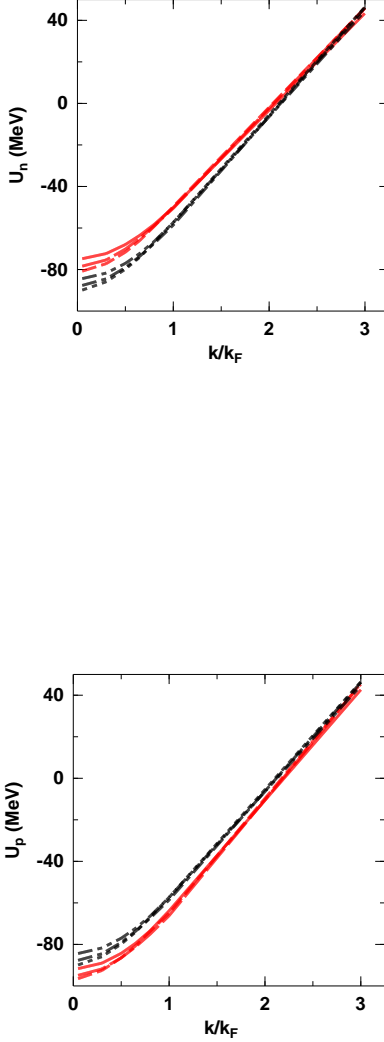


FIG. 10: (color online) Single-neutron (upper panel) and single-proton (lower panel) potentials *vs.* momentum (in units of the Fermi momentum, which is equal to  $1.4 fm^{-1}$ ). In the upper panel, the three higher curves are the predictions for  $\alpha=0.3$  at  $T=0$  (short dash),  $T=10$  MeV (long dash), and  $T=20$  MeV (solid). The three lower curves are the predictions in isospin symmetric matter at the same temperatures. The predictions become more repulsive with increasing temperature, as it can be best seen at the lowest momenta. In the lower panel, the predictions for the  $\alpha=0.3$  case are below those corresponding to  $\alpha=0$ .

where  $\tau, \tau' = n$  or  $p$ . The normalization condition, for each type of nucleon, becomes:

$$\rho_\tau = 2 \frac{1}{(2\pi)^3} \int_0^\infty n_{FD,\tau}(k, \rho, \alpha, T) d^3k. \quad (15)$$

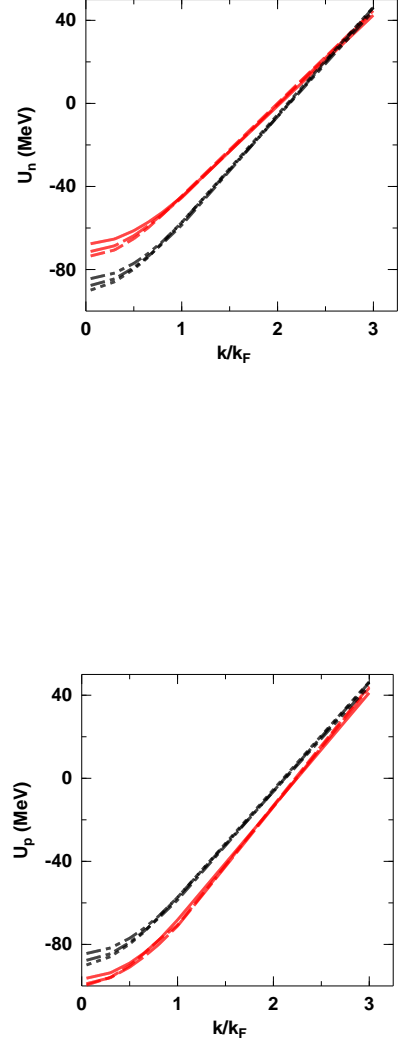


FIG. 11: (color online) Similar to Fig. 10, but for  $\alpha=0.5$ .

Similarly, the single-proton or neutron potentials become

$$U_\tau(\vec{k}, \rho, \alpha, T) = \sum_{\tau'} U_{\tau\tau'}, \quad (16)$$

where each  $U_{\tau\tau'}$  piece refers to a particular type of nucleon, and thus looks like Eq. (5) without the summation over isospin states. The calculation then proceeds to determine, self-consistently, the parameters of both protons and neutrons.

In Figs. 10-11, we show a representative set of results for the single-neutron and proton potentials. In both figures, the total density corresponds to an average Fermi momentum equal to  $1.4 fm^{-1}$ . The asymmetry parameter is equal to 0.3 and 0.5 in Fig. 10 and Fig. 11, respectively. The upper (lower) panel displays

the neutron (proton) potential. The potentials are displayed as a function of the momentum (in units of the Fermi momentum) for three different temperatures. For the neutron case, the three lower curves correspond to  $\alpha=0$ , whereas the three upper ones are the predictions for  $\alpha=0.3$ . In both sets, the potential becomes slightly more repulsive with increasing temperature, something which is noticeable only at the lowest momenta, as observed previously. For the proton case, similar considerations apply concerning temperature effects, but here the  $\alpha=0$  potentials are above the  $\alpha=0.3$  predictions. Figure 11 displays a similar scenario, but for  $\alpha=0.5$ . Thus, Figs. 10-11 show the effect of isospin asymmetry at each temperature. As expected [27], the neutron and the proton potentials “move away” from the symmetric matter predictions in opposite directions. The effect of isospin asymmetry is larger than the one of temperature.

#### IV. SUMMARY AND CONCLUSIONS

We used the Dirac-Brueckner-Hartree-Fock method extended to finite temperatures to predict single-particle properties in hot SNM and IANM. For temperatures up to a few tens of MeV the effect of temperature is small except at low densities and momenta. Due to suppression of Pauli blocking, which is most important at low momentum, some temperature-induced modification of (low-energy) in-medium cross sections could be expected.

This is an interesting point we will explore in future work. We also discussed the entropy/particle. When compared with other predictions in the literature, our results confirm the weak model dependence of this quantity.

As usual, we adopt the microscopic approach for our nuclear matter calculations. Concerning our many-body method, we find DBHF to be a good starting point to look beyond the ground state of nuclear matter, which it describes successfully. The main strength of this method is its inherent ability to effectively incorporate crucial TBF contributions [27] yet avoiding the possibility of inconsistency between the parameters of the two- and three-body systems.

We have focussed on the one-body properties of the system, which are of great relevance for the study of energetic heavy-ion collision dynamics. The extension of our isospin-asymmetric nuclear matter calculation, initiated in Ref. [26] and finalized in Ref. [27], to include the effect of finite temperature will enable us to consider additional aspects such as, for instance, proton fraction in hot beta-stable matter.

#### Acknowledgments

Support from the U.S. Department of Energy under Grant No. DE-FG02-03ER41270 is acknowledged.

- 
- [1] B.-A. Li, P. Danielewicz, and W. Lynch, *Phys. Rev. C* **71**, 054603 (2005).
  - [2] W. Zuo, Z.H. Li, A. Li, and G.C. Lu, arXiv:nucl-th/0412100, and references therein.
  - [3] L. Satpathy, M. Mishra, and R. Nayak, *Phys. Rev. C* **39**, 162 (1989).
  - [4] H.R. Jaqaman, A.Z. Mekjian, and L. Zamick, *Phys. Rev. C* **27**, 2782 (1983); R.K. Su, S.D. Yang, and T.T.S. Kuo, *Phys. Rev. C* **35**, 1539 (1987).
  - [5] M. Baldo, I. Bombaci, L.S. Ferreira, and U. Lombardo, *Nucl. Phys. A* **583**, 599c (1995).
  - [6] H.R. Jaqaman, A.Z. Mekjian, and L. Zamick, *Phys. Rev. C* **29**, 2067 (1984).
  - [7] B. ter Haar and R. Malfliet, *Phys. Rep.* **149**, 207 (1987).
  - [8] H. Huber, F. Weber, and M.K. Weigel, *Phys. Rev. C* **57**, 3484 (1998).
  - [9] A. Rios, A. Polls, and I. Vidaña, *Phys. Rev. C* **71**, 055802 (2005).
  - [10] I. Bombaci, A. Polls, A. Ramos, A. Rios, and I. Vidaña, *Phys. Lett. B* **632**, 638 (2006).
  - [11] R.B. Wiringa, V.G.J. Stocks, and R. Schiavilla, *Phys. Rev. C* **51**, 38 (1995).
  - [12] D. Lopez-Val, A. Rios, A. Polls, and I. Vidaña, *Phys. Rev. C* **74**, 068801 (2006).
  - [13] M. Baldo and L.S. Ferreira, *Phys. Rev. C* **59**, 682 (1999).
  - [14] T. Frick and H. Mütter, *Phys. Rev. C* **68**, 034310 (2003).
  - [15] M. Prakash, I. Bombaci, P.J. Ellis, J.M. Lattimer, and R. Knorren, *Phys. Rep.* **280**, 1 (1997).
  - [16] B.D. Serot and J.D. Walecka, *Adv. Nucl. Phys.* **16**, 1 (1986).
  - [17] B.D. Serot, *Rep. Prog. Phys.* **55**, 1855 (1992), and references therein.
  - [18] B.M. Waldhauser, J. Thesis, J.A. Maruhn, H. Stöcker, and W. Greiner, *Phys. Rev. C* **36**, 1019 (1987).
  - [19] H. Müller and B.D. Serot, *Phys. Rev. C* **52**, 2072 (1995), and references therein.
  - [20] N.K. Glendenning, *Nucl. Phys. A* **469**, 600 (1987).
  - [21] F. Weber and M.K. Weigel, *Z. Phys. A* **330**, 249 (1988).
  - [22] A. Rios, A. Polls, A. Ramos, and H. Mütter, *Phys. Rev. C* **74**, 054317 (2006).
  - [23] A. Rios, A. Polls, and I. Vidaña, *Phys. Rev. C* **79**, 025802 (2009).
  - [24] Ch. C. Moustakidis, *Phys. Rev. C* **78**, 054323 (2008).
  - [25] Ch. C. Moustakidis and C.P. Panos, *Phys. Rev. C* **79**, 045806 (2009).
  - [26] D. Alonso and F. Sammarruca, *Phys. Rev. C* **67**, 054301 (2003).
  - [27] F. Sammarruca, *International Journal of Modern Physics E*, in press; arXiv:1002.0146 [nucl-th].
  - [28] F. Sammarruca and P. Krastev, *Phys. Rev. C* **75**, 034315 (2007).
  - [29] R. Machleidt, *Adv. Nucl. Phys.* **19**, 189 (1989).
  - [30] R. Machleidt, F. Sammarruca, and Y. Song, *Phys. Rev. C* **53**, R1483 (1996).